13th International Symposium on Particle Image Velocimetry – ISPIV 2019
Munich, Germany, July 22-24, 2019

Flow-field analysis of subsonic jets at Mach 0.5 and 0.84 using 3D Multi-Pulse STB

Philipp Godbersen[1*], Peter Manovski[2], Matteo Novara[1], Daniel Schanz[1], Reinhard Geisler[1], Nagendra Karthik Depuru Mohan[3], Andreas Schröder[1]

[1] German Aerospace Center (DLR), Institute of Aerodynamics and Flow Technology, Göttingen, Germany

[2] Aerospace Division, Defence Science and Technology Group, Melbourne, Australia

[3] University of Cambridge, Cambridge, United Kingdom

[*] Philipp.Godbersen@dlr.de

Abstract

A subsonic air jet flow in air at Mach 0.506 and 0.845 generated by a round as well as a chevron nozzle with an inner diameter D_j of 15 mm is investigated using three-dimensional Lagrangian Particle Tracking and simultaneous far field microphone measurements. The Shake-The-Box (STB) method allows highly spatially resolved accurate velocity and acceleration measurements to be recovered at high particle densities when compared to a Particle Image Velocimetry (PIV) reference dataset. The high resolution is possible because of bin averaging the large amount of available snapshots and enables resolving extremely steep velocity gradients in the shear layer of the jet close to the nozzle. Mean velocity, acceleration and velocity fluctuation profiles as close as a distance of 0.2 D_j to the nozzle exit are presented. The density of recovered particles is sufficient for analysis of instantaneous tracks, velocity vector volumes, coherent structures, and evaluation of the velocity gradient tensor. Results are shown in terms of instantaneous visualizations of the flow-field in addition to the ensemble averaged statistics.

1 Introduction

The study of turbulent jet flow is a topic with long history in aerodynamic and aeroacoustic research. However to date only a limited number of experimental investigations using volumetric measurements have been conducted. One such study is conducted by Wernet (2016) who examines a Mach 0.9 jet using Tomographic PIV. They successfully capture the volumetric flow-field and make comparisons to the NASA consensus dataset by Bridges and Wernet (2011). While the Tomo-PIV measurements generally agree with the consensus data on the jet center line, they note that deviations are found in the shear layer and that the results appear to be sensitive towards high gradients in the flow. Especially in the shear layer close to the nozzle where the uncertainties are much greater. However this region is of high interest, the shear layer development in the very near nozzle region influences noise generation as well as turbulence statistics further downstream of the jet as shown by Fontaine et al. (2015).

This study expands on prior work by Manovski et al. (2018) and aims to provide further insight into the flow physics of subsonic jets by utilizing Lagrangian 3D particle tracking via the Shake-The-Box (STB, Schanz et al. (2016)) algorithm and subsequent data assimilation by FlowFit (Gesemann et al., 2016) to provide high resolution velocity, acceleration and pressure data. The original STB method relies on creating long particle tracks using time resolved measurements which requires relatively low speed flows. Due to the high velocities present in this investigation, the multi pulse variant as introduced by Novara et al. (2016a,b) is employed instead. The particle tracking approach has advantages over PIV based methods used in prior studies as it is not limited by the spatial low-pass filtering effect inherent in correlation based methods. The STB method allows for accurate particle tracking of densely seeded flows, allowing not just flow statistics to be captured but also consideration of instantaneous flow states as well.

The combination of the volumetric particle tracking with synchronized microphone measurements will provide further insight into the relationship between the dynamics of flow structures and noise generation

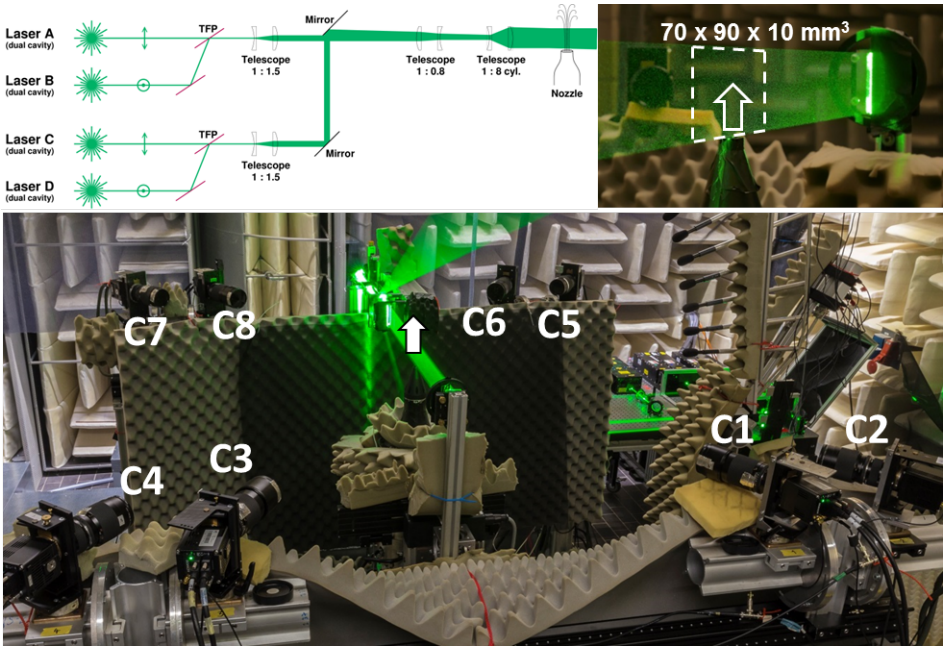

Figure 1: Pictures of the experiment setup showing the camera system arrangement and measurement volume. A diagram of the Illumination setup is provided in the top left corner

of the jet. A preliminary analysis of the microphone data of this experiment was conducted by Depuru Mohan et al. (2017) and shows the noise directivity of the jet flow. While this paper will focus on the tracking measurement, further work will include a combined analysis of the large statistical basis provided in this experiment. One such topic will be the use of causality correlation between velocity field values and microphone data as performed by Henning et al. (2013) using Stereo-PIV on a jet using the same nozzle as examined here.

2 Experimental Setup

The experiments were carried out in the Aeroacoustics Test Facility (SAG) at the German Aerospace Center (DLR) in Göttingen. Two different nozzle geometries, each with an inner diameter D_j of 15 mm and a lip thickness of 3 mm were investigated. A round nozzle as well as a chevron nozzle with six notches, both having an inner geometry described by a seventh order polynomial. A detailed description of both nozzles used is given by Miguel and Henning (2013). To accurately set the flow conditions of the jet (that is, nozzle pressure ratio and nozzle temperature) a differential pressure manometer (*Greisinger GDH-14A*) as well as a thermocouple (*8RS Pro Thermoelement Type K*) were used. Two different Mach numbers were investigated, M=0.506 and M=0.845. The nozzle is movable in the axial direction enabling different measurement positions along the jet axis. During the course of the experiment, three different positions were investigated, one being close to the nozzle, the other covering the end of the potential core and the last further downstream. The three positions are partially overlapping, allowing for full coverage from the nozzle up to $11D_j$ downstream. The volumetric flow-field of the jet was captured using the multi pulse variant of the STB technique as described by Novara et al. (2016a,b). A combination of two dual frame acquisition systems separated by polarization filters is used to capture images of tracer particles illuminated in a $90 \times 70 \times 10\,\mathrm{mm}^3$ volume using a 10 Hz frame rate. Illumination is provided by two dual-cavity BigSky Evergreen Nd:YAG lasers and two dual-cavity BigSky CFR400 Nd:YAG lasers emitting horizontal and vertical polarized light respectively. In order to increase the available laser energy each pulse of the Evergreen lasers is combined with one pulse of the CFR400 lasers resulting in a total energy per pulse of approximately 400 mJ with the whole system being capable of four pulses in quick succession. A schematic of the laser setup is given in Figure 1. The laser sheet was also back reflected in order further increase the available illumination and to even out image intensity variations on the camera images caused by the Mie scattering lobes. The timing scheme of the lasers is set up as a four pulse sequence where the time separation between pulses 1 and 2, and that between pulses 3 and 4

Table 1: STB processing parameters and jet flow data

Iteration	1	2	3	4
Triangulations with N_c	3	3	3	3
Triangulations with N_{c-1}	2	2	2	2
Shake iterations (IPR)	10	10	10	10
Shake width [px]	0.1	0.1	0.1	0.1
Allowed triangulation err. [px]	0.8	0.8	0.8	0.8
Global search radius δ_{2p} [px]	0.5	1.0	2	3
Search radius mult. factor $f_{\sigma,2p}$	2	3	3	4
Global search radius δ_{4p} [px]	0.7	1.5	3	4
Search radius mult. factor $f_{\sigma,4p}$	3	5	5	5

	Mach number	
	0.506	0.845
Exit axial velocity [$\mathrm{m\,s^{-1}}$]	173.77	290.57
Reynolds number (Re_{D_j})	1.7×10^5	3.1×10^5
Nozzle Pressure Ratio	1.19	1.71
Nozzle Temperature Ratio	1.0	0.98
Total 4-pulse sequences	45000	60000
Pulse delay 1-2 and 3-4 [µs]	2.25	1.25
Pulse delay 2-3 [µs]	6.75	3.75

is kept the same and a longer time interval separates pulses 2 and 3 (refer to Table 1). Using a fast sensing light diode and a oscilloscope the pulse timing and pulse overlap between lasers was confirmed to be within ±2 ns. The two imaging systems consist of four sCMOS PCO-Edge cameras each and are equipped with polarization filters to separate the laser pulses among the two systems. One imaging system (odd camera numbers) records pulses 1 and 2, and the other (even camera numbers) pulses 3 and 4. The camera positions are depicted in Figure 1. The sensor size is 2560×2160 pixel with an individual pixel size of 6.5 µm. The cameras in Scheimpflug condition are equipped with lenses having a focal length of 200 mm and 180 mm with an f-stop number of 11. The digital resolution was approximately 33.63 pixel/mm.

A Laskin nozzle with a separate impactor was used to provide seeding of Di-Ethyl-Hexyl-Sebacat (DEHS) with a nominal particle diameter of 1µm. The seeding was introduced upstream of the nozzle and the ambient air was also seeded enabling a near homogeneous distribution across the measurement volume. The seeding concentration adopted for the experiment resulted in a particle image density of approximately 0.015 to 0.04 ppp (particles per pixel). The imaging systems were calibrated using a LaVision Type-11 two-plane target and further refined with volume self calibration (VSC,Wieneke (2008)).

For the Mach 0.506 measurement configuration a total of 45000 four-pulse sequences were recorded at 10 Hz. Similarly for the Mach 0.845 measurement configuration a total of 60000 four-pulse sequences were recorded at the same frequency. Synchronously the far-field acoustic pressure fluctuations were recorded by a microphone array consisting of 17 microphones. Of these, 13 microphones were located in a polar array at approximately $60D_j$ arranged at angles 90° to 30° to the jets axial axis in 5° increments. The remaining 4 microphones were positioned at approximately $180D_j$ at angles 90°, 60°, 45° and 30° to the jets axial axis. The microphones were sampled using 250 kHz with a high pass filter at 500 Hz. Both the velocity and the pressure measurements were synchronized by the master clock of the data acquisition system (*ViperHDR*).

3 Shake-the-Box Processing

The captured image data is processed using the multi pulse variant of the Shake-The-Box method (Novara et al., 2016a,b) originally introduced by Schanz et al. (2016). Multi-pulse STB applies the concept originally conceived for determining long particle tracks from time resolved data to short tracks of just a few pulses. The method delivers tracks with a length of four pulses which can then be evaluated at their midpoint for values of velocity and material acceleration via a polynomial fit of the particle positions. The midpoint is chosen as it provides the best accuracy. In order to apply the method, careful calibration of the imaging system is necessary. The initial geometric calibration is refined by VSC on flow-off images with low seeding density. The flow-off condition allows the calibration of both systems together even though their pulse timings are different. For each change in experiment parameters and at the start of each day, a fresh calibration dataset was recorded. Through this approach, very low sub pixel disparities are reached and high quality empirical optical transfer functions (OTF, Schanz et al. (2012)) necessary for STB processing are extracted. To further increase the accuracy, run specific calibrations are created using a subset of the actual flow-on images of a run. For this the two systems need to be treated separately as both see different instants in time. Additionally, a vibration correction is applied by a global shake approach using the triangulated particles and the camera parameters for each individual flow-on snapshot, recovering small 2D shifts of the imaging planes. The camera calibration and OTF are used for the iterative particle reconstruction, determining the 3D particle positions for each pulse. At this stage, four particle clouds are available, one for each pulse. The tracking

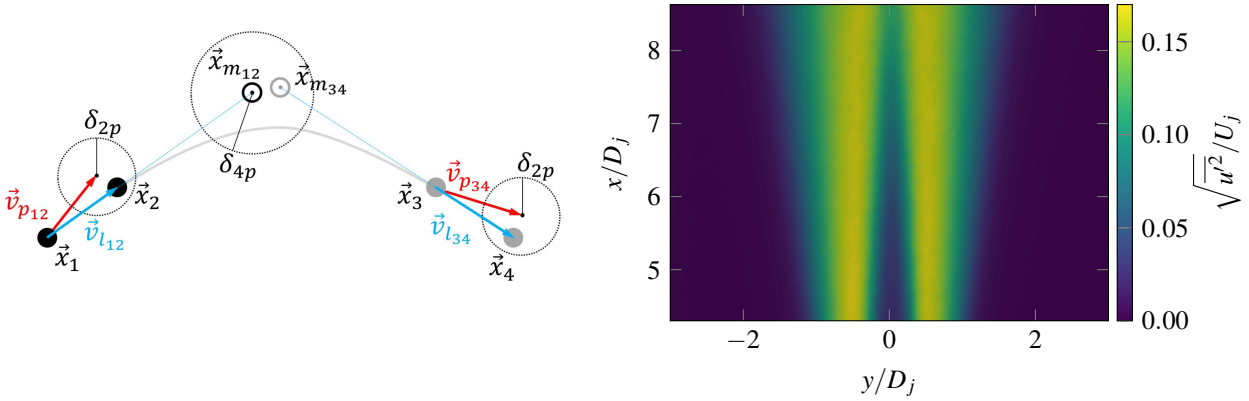

Figure 2: Left: Sketch of tracking strategy. Right: For tracking enhancement the standard deviation of the velocity calculated on a small subset of the available data was used. An example is shown here of the coarse bin averaged axial velocity standard deviation through the center of the jet.

strategy shown in Figure 2 (left) is separated into two stages. In a first step two pulse tracks are discovered between pulses 1 and 2, and 3 and 4. For each particle in the first pulse, matching particles are selected in the next pulse based on a search radius δ_{2p} and predictor values $\vec{v}_{p12}$ and $\vec{v}_{p34}$. In order to build four pulse tracks, the found two pulse tracks are extrapolated towards a common midpoint $\vec{x}_{m12}$ and $\vec{x}_{m34}$ and two pulse tracks are matched to each other by using the search radius δ_{4p}. The resulting four pulse track candidates are filtered with respect to duplicates and checked for validity resulting in the final four pulse tracks. Velocity and acceleration data can be obtained from a polynomial fit of the track positions.

Initial processing uses Particle Space Correlation (PSC, Novara et al. (2016a)) in order to derive a predictor field from the particle data prior to tracking. This predictor is the used in conjunction with fixed search radii. Such a configuration is used to process a subset of the data in order to enable a data driven approach for selecting predictors and search radii. The flow-field is characterized by a calm outer region, the highly turbulent shear layer and the potential core of the jet. Each of these regions benefit from different parameter settings. While the outer region allows for very small search radii as the flow is well characterized by a predictor, care must be taken to have sufficiently large search radii in the shear layer as high deviations from the predictor field are to be expected. This motivates the use of variable search radii whose size is scaled based on the local standard deviation of the velocity. The initial processing of a subset of the images is used to calculate the local mean and standard deviation using ensemble averaging of the track data. Figure 2 (right) shows an example of such a bin average. The averaging process is described in Section 3.1. During tracking, the provided mean field is queried for each particle and the two-pulse and four-pulse search radii set based on parametrized linear functions:

$$\delta^*_{2p} = \delta_{2p} + f_{\sigma,2p}\,\sigma, \qquad \delta^*_{4p} = \delta_{4p} + f_{\sigma,4p}\,\sigma, \tag{1}$$

with the adapted search radius δ^*_{2p}, a fixed global base radius δ_{2p}, a multiplication factor $f_{\sigma,2p}$ and the local standard deviation of the velocity σ. These equations are evaluated for a vector valued $\sigma = [\sigma_x, \sigma_y, \sigma_z]$, resulting in an anisotropic search radius in accordance with the velocity fluctuation in each coordinate direction. For the four-pulse search radius the use of the standard deviation of acceleration would be more appropriate but it is not available with sufficient quality at this stage as only a small subset of snapshots is used. For the turbulent flow considered here high accelerations are only expected in the shear layer where the velocity fluctuations are also high, making the use of velocity a valid simplification. However this is not necessarily the case for all flows.

An overview of the used STB parameters is given in table 1. Using this setup, between 40 000 and 100 000 tracks are recovered per snapshot, depending on seeding density and image quality. As the scattering intensity not only depends on the viewing angle but also on the polarization direction of the light, particles are not always sufficiently imaged on both systems. This can lead to situations where no matching partner can be found in the other system even though the particle is triangulated correctly, causing missing tracks. Novara et al. (2019) discuss this effect in greater detail and provide comparisons to different acquisition strategies which are not based on polarization. They suggest that a multi-exposure strategy would result in less tracks lost and therefore a better reduction of residual images.

3.1 Bin Averaging and Post-processing

The short tracks recovered by the multi-pulse STB technique are especially well suited for high resolution turbulence statistics as each particle carries very accurate velocity information without any of the windowing effects inherent in PIV measurements. The scattered nature of the track positions makes it necessary to average over spatial volumetric bins but their size can be freely set during post processing according to the convergence needs of the chosen statistic. Since the particle positions between the separate snapshots are essentially random, additional snapshots increase the particle density during ensemble averaging. Increasing the amount of snapshots therefore increases the possible spatial resolution when bin averaging the data. This allows for a convergence/resolution trade-off where the bin size is set as small as possible while still allowing for convergence of the considered statistic. Such considerations could also drive the positioning and size of adaptive bins but this is not yet considered in the evaluations presented here. Additional resolution can be gained by also including further assumptions like the axis symmetry of the jet.

The large amount of snapshots collected allows further correction of already small errors in the measurement setup by including physics based assumptions on the flow-field. The initial timing of the laser pulses was measured to be within a couple nanoseconds of each other but small differences still remain. Since the acceleration is calculated from the second derivative of the position with respect to time, it is very sensitive to slight deviations of the pulse timings. As the mean acceleration in the center of the jet close to the nozzle within the potential core is supposed to be zero, this can be enforced in the measured data by introducing a small correction to the given pulse timings. Similar considerations can be made to correct small calibration errors between the two camera systems. During calibration the two systems were calibrated separately during fine-tuning leaving the possibility of slight misalignments of the two systems to each other. This can be corrected in a similar matter to the time pulse correction by analyzing the mean acceleration in the outer regions and introducing a spatial offset between the two camera systems. The calculated correction values are very small, in the region of a hundredths of a pixel for the calibration correction and less than a nanosecond for the timing adjustment.

4 Results

Figure 3 shows an overview of the instantaneous particle tracks recovered for the different jet configurations. For these visualizations, the snapshots at the different measurement positions have been combined together in order to give an overall impression of the extent of the measurement range and the flow-field. These snapshots do not correspond to the same instant in time. The figures have been truncated in the radial direction for better display, the actual measurement space extends more than three nozzle diameters to each radial side. Both jet configurations with the round nozzle are captured up to eleven nozzle diameters in the axial direction while the chevron variants reach up to nine. Differences between the two nozzle types are immediately apparent, with the chevron nozzle having a much shorter potential core along with a thicker shear layer. Figure 4 (left) shows the decay of the centerline axial velocity for the Mach 0.845 jet with the round nozzle showing the transition into a linear decay after the end of the potential core. Further insights are gained by processing the instantaneous tracks with the FowFit algorithm described by Gesemann et al. (2016). FlowFit provides a continuous B-spline basis for flow quantities via a physics based data assimilation approach. Among the velocity, acceleration and pressure fields, this also provides access to the velocity gradient tensor and associated vortex criteria. Figure 4 (right) shows isocontour surfaces of the Q-criterion for the Mach 0.506 jet with the round nozzle extracted through this approach. The outer region of the jet is shown, after the end of the potential core. This is evident in the visible vortex structures extending into the center of the jet.

The high particle density combined with a large number of snapshots allows the investigation of bin averages with very high resolutions. Figure 5 shows the results of a bin averaging using a size of 0.75 px in comparison to the PIV results of NASA consensus dataset by Bridges and Wernet (2011). Although test conditions differ it still provides a good reference for comparisons, especially with respect to the quality of the respective measurement techniques. For $x/D_j = 1$ both measurements resolve the mean axial velocity profile well but differences are visible for the fluctuations. The STB method shows a lower noise floor in the outer region and the potential core. It also predicts higher values in the shear layer with sharper peaks. This may be attributed to the higher spatial resolution and accuracy of the Lagrangian particle tracking method where no spatial filtering is introduced. To highlight the STB methods ability to resolve very thin shear layers the profiles at $x/D_j = 0.2$ are also shown. The steep velocity gradient appears to be well resolved. In addition to the velocities, the STB measurement allows examination of acceleration profiles as well. Fluid is accelerated towards the shear layer from the inside as well as the outside of the jet. The acceleration profiles extend slightly further than the top hat form of the velocity profiles showing the influence of vortices forming on the

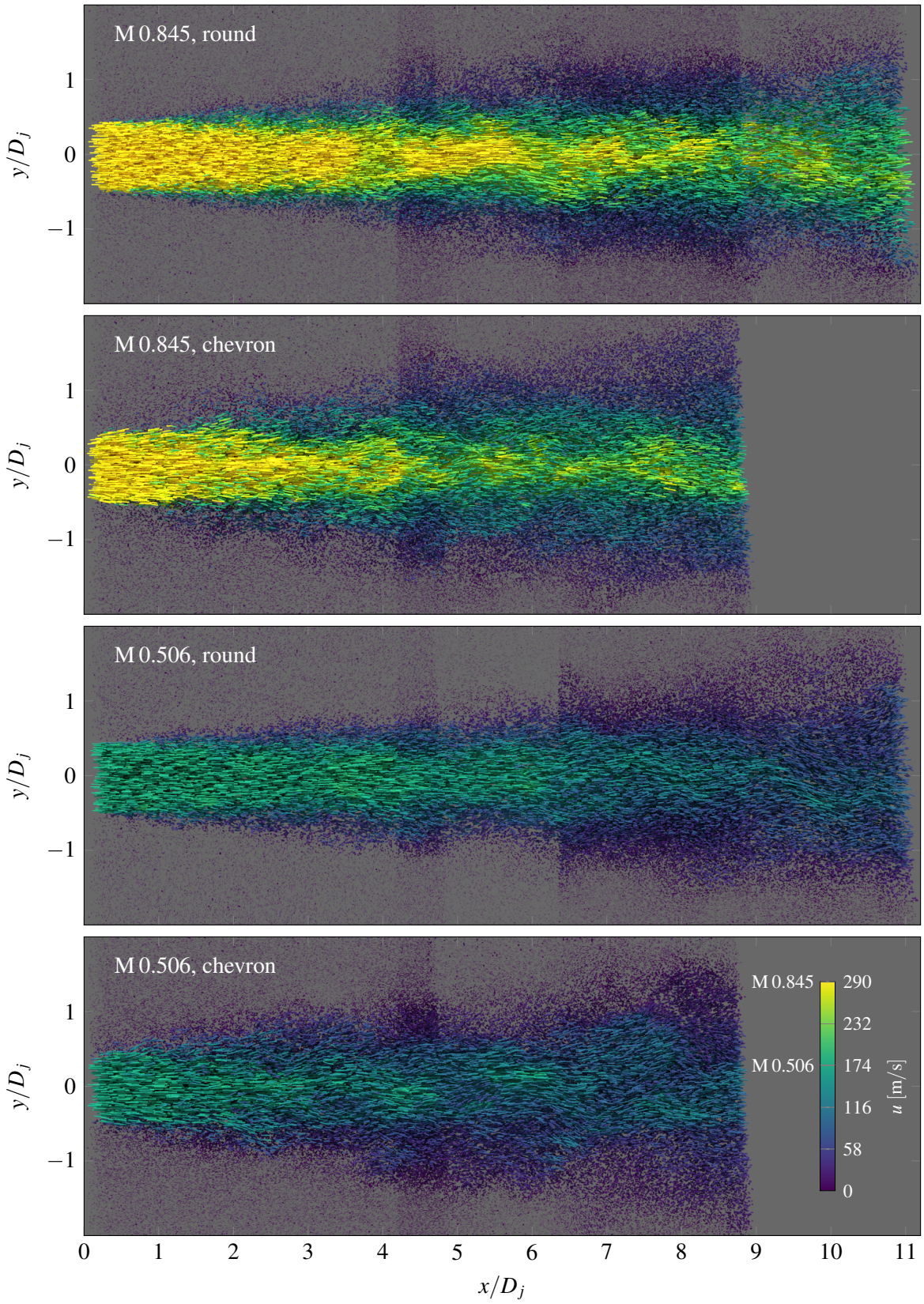

Figure 3: Montage of instantaneous tracks colored by axial velocity

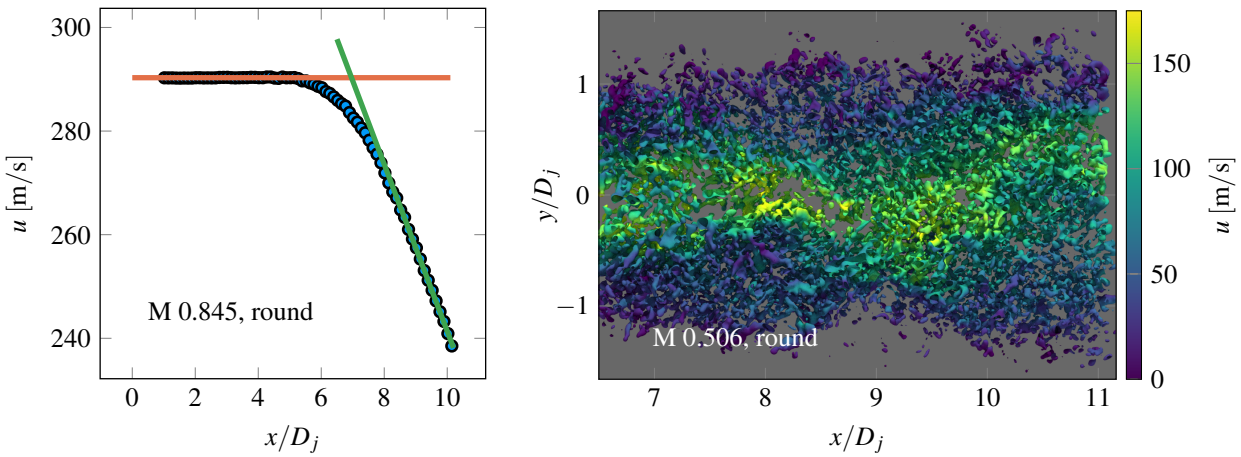

Figure 4: Left: Axial velocity decay along the center line for the Mach 0.845 jet with the round nozzle calculated using a small subset of the available data. Right: Isocontour surfaces of the Q-criterion for the Mach 0.5 jet with the round nozzle from a flow fit at the outer measurement position colored by axial velocity.

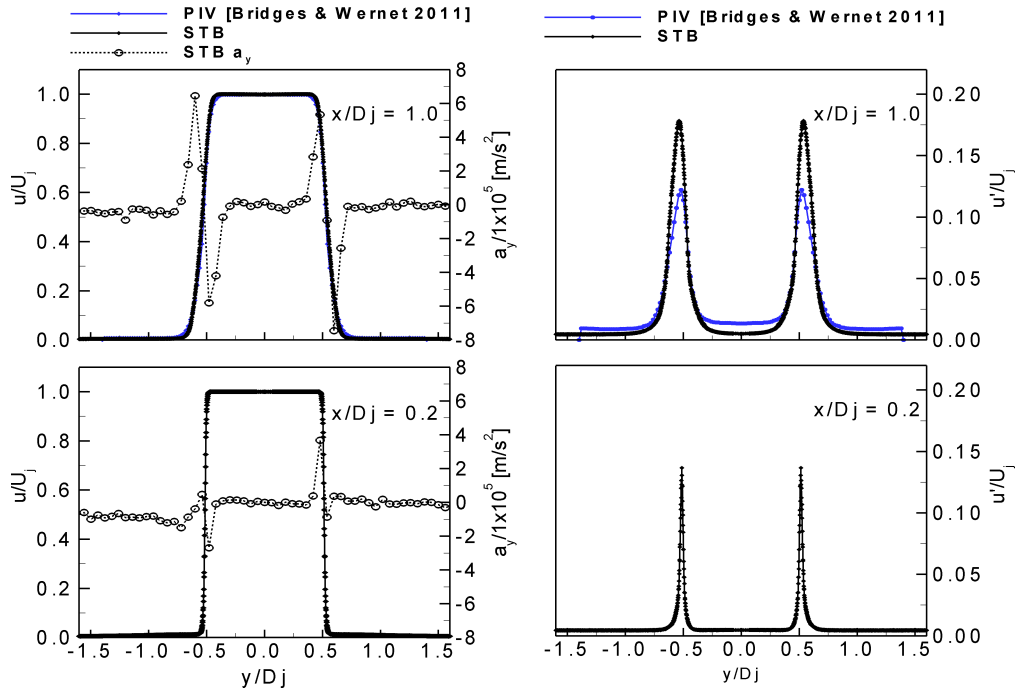

Figure 5: STB velocity and acceleration profiles including a comparison with the NASA consensus data (Bridges and Wernet, 2011).

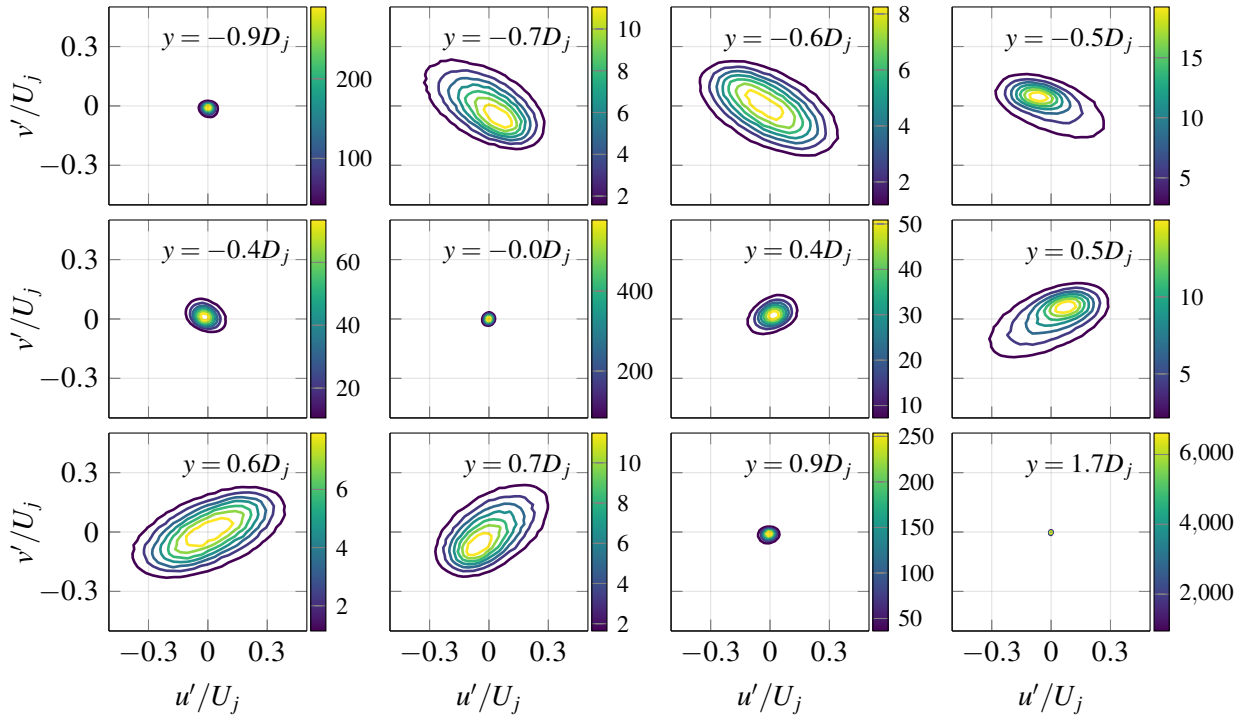

Figure 6: Joint probability density functions of u' and v' evaluated at various points along the line $(45\,\text{mm}, y, 0\,\text{mm})$ at approx. $3D_j$ downstream. The statistics were calculated in a bin with size $2\times1\times1$ mm^3 around each point.

interface. The acceleration data is noisier than the velocity profiles due to their greater sensitivity towards errors in tracking accuracy and the relatively low dynamic range. The profiles shown here were generated using an older evaluation of the experiment. Future work will benefit from algorithmic improvements and evaluation of the full dataset. An analysis of the accuracy of the current evaluation algorithm is conducted by Novara et al. (2019).

In addition to the profiles the tracks also allow to calculate probability densities (PDF) of the velocity fluctuations in axial and radial directions. These are determined in a similar bin averaging approach at various points in the flow. Figure 6 shows a selection of joint PDFs evaluated along a line across the center of the Mach 0.845 jet with the round nozzle at $x/D_j = 3$ with a bin size of $2\times1\times1$ mm^3. The points are symmetric about the origin from $y = -0.9D_j$ to $y = 0.9D_j$ with an additional point at $y = 1.7D_j$. The additional point was chosen as the endpoints of the line are within in shear layer of the jet. Within the shear layer the PDFs present as diagonally oriented ellipses, associating positive axial fluctuations with positive radial fluctuations.

5 Conclusion and Outlook

The multi-pulse STB method provides highly resolved velocity and acceleration measurements at high particle densities. The amount of recovered tracks allows not just for ensemble averaging over a large amount of snapshots, but also to investigate the instantaneous velocity fields. Combining the separate measurement positions allows for high resolution visualization of the jet flow. The large number of snapshots acquired during the experiment makes it possible to calculate extremely high resolved flow statistics via bin averages of the tracked particles. This allows the even extremely thin shear layers with steep velocity gradients near the nozzle exit to be resolved. The comparison with the PIV based consensus dataset by Bridges and Wernet (2011) show the superiority of Lagrangian particle tracking over correlation based methods when calculating flow statistics. The PIV technique suffers from spatial low-pass filtering effects as it is a windowing based method and for extremely fine features is unable to resolve them at all. The STB method requires a high amount of care in calibrating the imaging system and timing the laser pulses. The measurement of acceleration is very sensitive to these input variables, especially the pulse timing. However corrections can be made during

post-processing if necessary. For the current work, only a partial evaluation of all the recorded snapshots was available. Future work will include a full processing of all available jet configurations enabling for comparisons using the full amount of data. The scattered track positions combined with the binning approach allow for a virtual measurement probe for high quality bias free statistics to be placed anywhere in the measurement volume. This facilitates further statistical analysis using probability density functions, two point statistics and conditional averaging. For cases with very high seeding density analysis of the terms of the turbulent kinetic energy equation, including the dissipation rate, might be possible. One large aspect yet to be explored is the combined analysis of the tracking and acoustic measurements. The volumetric nature of the STB data provides ample opportunity for investigating noise generating structures within the jet in three dimensions. As the two dimensional causality correlation study by Henning et al. (2013) using Stereo-PIV was performed on the identical jet setup it is suitable as reference for further investigations. The processing of instantaneous track data with FlowFit (Gesemann et al., 2016) provides the measurement data as a continuous representation on a regular grid. This enables direct access to the velocity gradient tensor and also allows for the use of modal decompositions in the analysis which is not possible on the scattered particle data. It also provides the instantaneous pressure fields which are of prime interest for jointly analyzing the microphone and flow measurements.

Acknowledgements

The present work has been partially funded by the DFG-project "*Analyse turbulenter Grenzschichten mit Druckgradient bei großen Reynolds-Zahlen mit hochauflösenden Vielkameramessverfahren*". Computer resources for this project have been provided by the Gauss Centre for Supercomputing/Leibniz Supercomputing Centre under grant: pr62zi. Dr. Depuru Mohan would like to thank the Government of Germany for the award of a DLR-DAAD Research Fellowship to perform this work at the German Aerospace Center (DLR), Göttingen.

References

Bridges J and Wernet MP (2011) *The NASA subsonic jet particle image velocimetry (PIV) dataset*. National Aeronautics and Space Administration, Glenn Research Center

Depuru Mohan NK, Manovski P, Geisler R, Agocs J, Ahlefeldt T, Novara M, Schanz D, Haxter S, Ernst D, Spehr C, and Schröder A (2017) Aeroacoustic analysis of a Mach 0.9 round jet using synchronized microphone array and Shake-The-Box 3D Lagrangian particle tracking measurements. in *23rd AIAA/CEAS Aeroacoustics Conference*. page 3862. American Institute of Aeronautics and Astronautics

Fontaine RA, Elliott GS, Austin JM, and Freund JB (2015) Very near-nozzle shear-layer turbulence and jet noise. *Journal of Fluid Mechanics* 770:27–51

Gesemann S, Huhn F, Schanz D, and Schröder A (2016) From noisy particle tracks to velocity and acceleration and pressure fields and using b-splines and penalties. in *18th International Symposium on the Application of Laser and Imaging Techniques to Fluid Mechanics*. pages 2684–2700

Henning A, Koop L, and Schröder A (2013) Causality correlation analysis on a cold jet by means of simultaneous particle image velocimetry and microphone measurements. *Journal of Sound and Vibration* 332:3148–3162

Manovski P, Novara M, Depuru Mohan NK, Geisler R, Schanz D, Agocs J, and Schröder A (2018) 3D Lagrangian Particle Tracking of a high-subsonic jet using four-pulse Shake-The-Box. in *Applications: Volumetric Measurements in Particle Image Velocimetry: A practical Guide*. pages 616–622. Raffel et al., 3rd edition, April 2018.

Miguel E and Henning A (2013) Analysis of simultaneous measurement of acoustic pressure in the far-field and density gradient in the near-field in a cold jet. in *19th AIAA/CEAS Aeroacoustics Conference*. page 2034. American Institute of Aeronautics and Astronautics

Novara M, Schanz D, Geisler R, Gesemann S, Voss C, and Schröder A (2019) Multi-exposed recordings for 3d lagrangian particle tracking with multi-pulse shake-the-box. *Experiments in Fluids* 60:44

Novara M, Schanz D, Gesemann S, Lynch K, and Schröder A (2016a) Lagrangian 3D particle tracking for multi-pulse systems: performance assessment and application of Shake-The-Box. in *18th International Symposium on the Application of Laser and Imaging Techniques to Fluid Mechanics*. pages 2638–2663

Novara M, Schanz D, Reuther N, Kähler CJ, and Schröder A (2016b) Lagrangian 3d particle tracking in high-speed flows: Shake-the-box for multi-pulse systems. *Experiments in Fluids* 57:128

Schanz D, Gesemann S, Schröder A, Wieneke B, and Novara M (2012) Non-uniform optical transfer functions in particle imaging: calibration and application to tomographic reconstruction. *Measurement Science and Technology* 24:024009

Schanz D, Gesemann S, and Schröder A (2016) Shake-the-box: Lagrangian particle tracking at high particle image densities. *Experiments in Fluids* 57:70

Wernet MP (2016) Application of tomo-piv in a large-scale supersonic jet flow facility. *Experiments in Fluids* 57:144

Wieneke B (2008) Volume self-calibration for 3D particle image velocimetry. *Experiments in Fluids* 45:549–556